A Transformerless Photovoltaic System Employing a Cubic Cell Boost Converter for Low Voltage Application

Anjana Saikia and Santanu Sharma*
Department of Electronics and Communication Engineering, Tezpur University, Tezpur, India
Email: anjana.saikia113@gmail.com (A.S.), santanu.sharma@gmail.com (S.S.)

***Abstract*—A photovoltaic (PV) system is commonly used to satisfy the power demand of the utility. This paper investigates the utilization of a high voltage gain Cubic Cell Boost Converter (CCBC) in a transformerless photovoltaic (PV) system for low voltage applications. The proposed system is a combination of a CCBC and a three-phase inverter creating a two-stage three-phase PV system. The CCBC is linked with the low-scale PV sources to step up its input DC voltage and maintain a constant DC bus voltage by employing the Perturb and Observe (P&O) Maximum Power Point Tracking (MPPT) control algorithm. The DC bus is further connected to an LCL filter based three-phase inverter using a synchronous reference frame (*dq*) control scheme to power the three-phase utility. The proposed combination is validated by simulating in MATLAB/ SIMULINK environment for a 5.5 kW PV source and achieved an efficiency of 91% with 1.91% of inverter Total Harmonic Distortion (THD) at unity power factor. In the proposed system, CCBC with P&O MPPT control provides a high step-up DC bus voltage with less input current ripple and output voltage ripple and maintains a constant DC bus under variable solar irradiance. This work does not account for the common leakage current that is often produced in a transformerless PV system.**

***Index Terms*—*dq* control, inverter THD, perturb and observe (P&O), photovoltaic, ripple, transformerless system**

I. Introduction

Renewable energy sources are an inadequate solution to fulfill the world's energy crisis which is constantly growing with the increasing population rate. Moreover, renewable energies are clean energy sources that have zero emissions of greenhouse gases to the environment. Consequently, non-conventional energy sources are being extensively researched in the discipline of power electronics to improve their technology and cost-effectiveness. Most grid inverters (GI) commonly have two stages: a DC-DC converter stage and an inverter stage where conventional DC-DC power converters are commonly used to adjust the output voltage or current concerning the input side requirement of the inverter [1]. An inverter is used in the PV system to invert the DC output of the PV panel or the DC-DC converter into a synchronized sinusoidal waveform to send it to the grid. The GI topologies used in PV applications can be categorized as following [2]:

1) Single-stage inverter: In this topology, one grid-connected inverter controls the grid-current single-handedly.
2) Dual-stage inverter: In this topology, there are two stages i.e., a DC-DC stage and an inverter (DC-AC) stage. The first stage works based on MPPT control and the second stage i.e., the inverter performs the grid current control.
3) Multistage inverter: In this topology, various DC-DC converters are connected to one inverter.

PV arrays are affected by various environmental factors such as variable irradiance, ambient temperature, wind velocity, soiling, etc. which can lead to inconsistent DC output. DC-DC converter is commonly employed to carry on a stable DC-bus voltage for the system. To get optimized power in every instant an MPPT controller is used with the DC-DC converter. In a two stage Photovoltaic system, numerous topologies on DC-DC converters are commonly used with the GIs to transmit power to the utility. A DC-DC stage used with GI shows a controlled DC bus voltage at a lower level, and hence it is viable to design with a reduction of filter size than the filter designed for the full MPPT voltage while maintaining good system efficiency. Back to the literature, Merai *et al.* [3] proposes a design methodology to control DC-link voltage for a single-phase PV system with different configurations. In [4], step-up grid-connected double-stage PV inverter and its control approaches are explained. A grid-connected modular multilevel converter and a balanced three-phase system for large-scale PV applications have been illustrated in [5]. A three-phase grid-tied PV system analysis for a sinusoidal improved dual-stage inverter is implemented in [6] to handle the phase imbalances using a low-power DC-DC converter. In [7], a voltage control of a boost converter with floating interleaved technology for a fuel cell system has been implemented and validated with a 100W prototype converter. For an enhanced voltage gain, a Z-source converter-based system is explained in [8] for PV applications. In [9], a hybrid multilevel two-stage grid-connected DC/DC converter topology utilizing SiC devices introducing zero voltage switching (ZVS) is implemented.

Manuscript received September 15, 2023; revised November 20, 2023; accepted December 15, 2023.
*Corresponding author

A DC-DC high voltage gain converter is generally preferred in renewable energy applications to step up the source voltage level to kilo volts. In [10], a flying-capacitor-based multilevel boost converter is implemented employing reduced passive elements in the circuit with a DC voltage gain equal to the conventional boost converter. A DC-DC boost converter is modified with an algebraic series parallel switched capacitor for wide input voltage with enhanced power density [11]. A combination of a high step up cubic voltage multiplier cell boost converter combined with a switched capacitor to reduce voltage stress has been introduced in [12]. The cubic cell boost converter can be applicable for low and medium PV applications as it has significantly high DC voltage gain and the lesser numbers of passive and switching elements make the converter compact and lower in voltage stress and conduction loss. As the PV energy depends on solar irradiance and fluctuates under different environments, to receive maximum and stable output from the fluctuating PV array, a closed loop control along with the MPPT technique can be used. Ref. [13] states an interleaved multilevel converter with a voltage multiplier cell implemented for step-up applications. A three-phase two-stage PV inverter with SEPIC and CUK converter is explained in [14] for large-scale PV applications. In PV applications GIs are used to serve AC utility. In [15] a quasi-z source inverter is introduced for a single-stage PV application. A modified multilevel inverter with a fuzzy logic controller is explained in [16]. A model predictive controller is used for three-phase GIs [17]. An optimal *dq* control for three-phase GI is explained in [18] and [19] for low and medium PV applications. A general block diagram of a conventional two stage three phase PV system is explained in Fig. 1.

This paper proposes a 5.5 kW two-stage PV system with a combination of a high gain Cubic voltage multiplier cell as mentioned in [12] modified with conventional boost topology (CCBC) and a conventional 3-ph inverter. This system is an alternative solution for distributed GIs employed in small and medium-sized PV applications. The proposed combination involves PV arrays serving as a renewable energy source, a CCBC, and a 3-ph full bridge inverter using an LCL filter and *dq* control scheme to shape the voltage and feed the grid. The PV panel is connected to the CCBC to step up the PV voltage. The maximum power is drawn out from the PV panels even under variable irradiance adopting a P&O MPPT controller and the DC bus voltage is maintained by the PI controller connected with the MPPT controller. The proposed combination aims to provide an alternative scheme for low (<10 kW) and medium-scale (<500 kW) PV applications with higher conversion efficiency, lower input current and output voltage ripple and a robust control on DC bus voltage with lower inverter THD. Fig. 2 displays the complete circuit diagram for the proposed two-stage three-phase PV system combination showing the control schemes that have been implemented with the CCBC and the inverter topology.

This paper is structured as: Section II explains the circuit topology of the CCBC along with the MPPT algorithm. In Section III, inverter operation and its control have been discussed. Section IV explains system simulation and its results followed by the conclusion and future work of Section V.

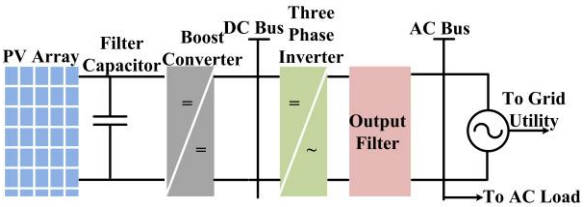

Fig. 1. Block diagram of a three phase PV system with two stage combination.

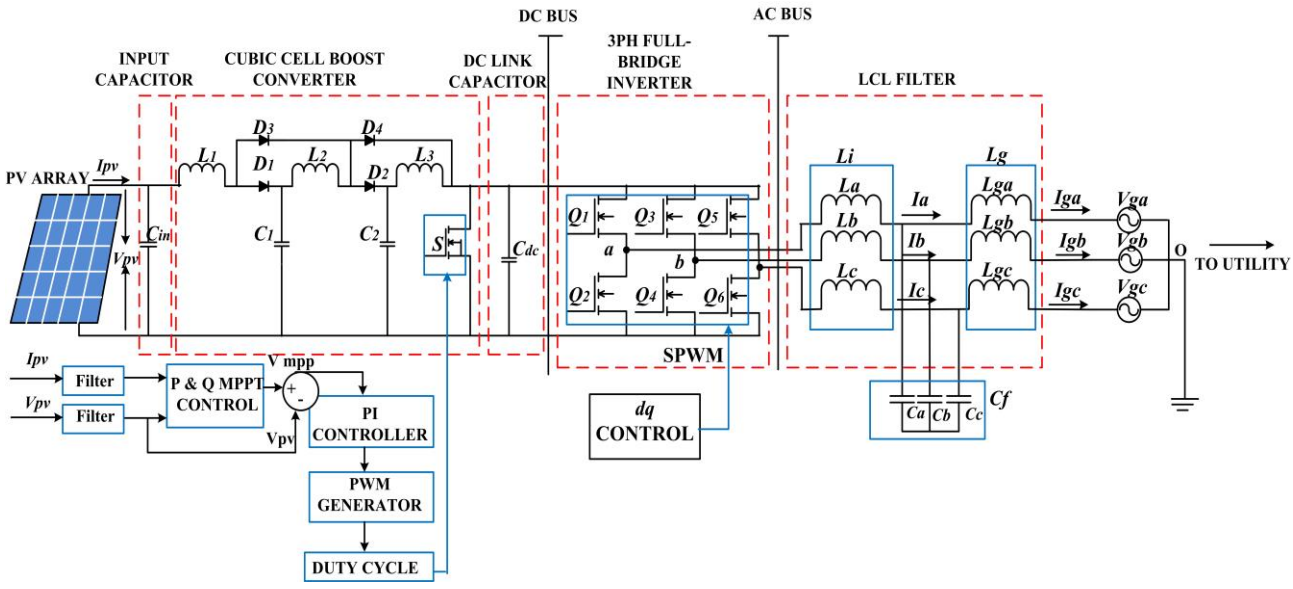

Fig. 2. Circuit design of the proposed two stage combination for a three-phase PV system.

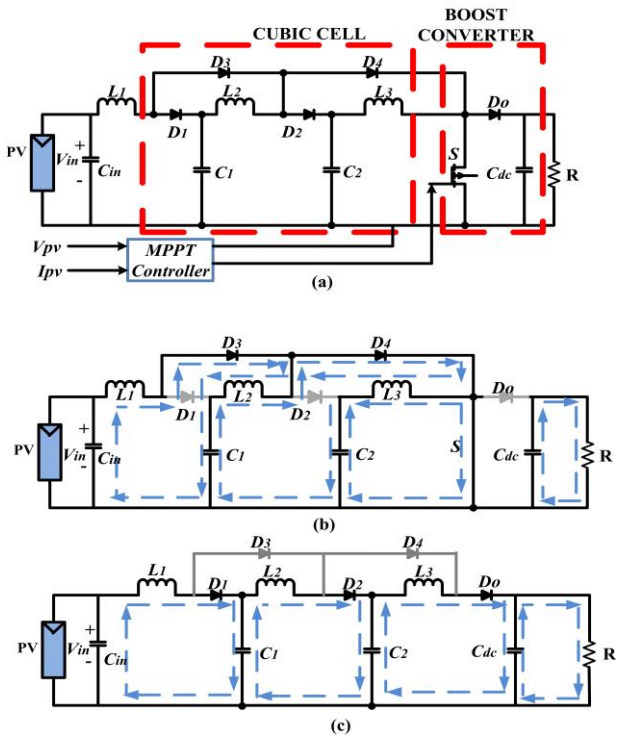

Fig. 3. Circuit diagram: (a) Cubic Cell Boost Converter (CCBC) (b) CCBC during switch ON mode (c) CCBC during switch OFF mode.

II. The Cubic Cell Boost Converter Analysis

Fig. 3(a) shows the circuit diagram of CCBC used in the proposed combination for the two stage three phase PV system. This converter is a modification of a cubic voltage multiplier cell consisting of three inductors, two capacitors, and four diodes with a conventional boost converter. The passive components of the CCBC are labeled as the inductors L_1, L_2, L_3, capacitors C_{in}, C_1, C_2, C_{dc} and the diodes D_1 D_2, D_3, D_4 and D_0. The inductor L_1 is the input inductor for the CCBC and D_0 is the output diode, C_{dc} is the output capacitor connected to the inverter input and works as a DC link capacitor providing DC bus voltage for the proposed combination. The CCBC is fed PV energy through the input capacitor C_{in} with input voltage V_{in}. Let, V_0 be the output voltage across the resistive load R assumed to explain the DC operation of the CCBC.

A. Circuit Topology

The switch S involves two working modes: switch ON mode and switch OFF mode as shown in Fig. 3(b) and (c) respectively. When S is turned ON, the input capacitor C_{in} is discharging with the DC input voltage V_{in} to the input inductor L_1 and hence L_1 starts charging. Meanwhile, during this period, the capacitors C_1 and C_2 are in discharging mode and they start to charge the corresponding inductors L_2 and L_3. Hence the diodes D_3 and D_4 carry forward bias voltage, and D_1, D_2 and D_0 carry the reverse voltage. In this period the stored energy of the output capacitor C_{dc} provides voltage V_0 to load R. From Fig. 3(b) during switch ON mode, applying KVL in the circuit, the voltage on each inductor is calculated separately as follows:

$$V_{in} = V_{L_1} \tag{1}$$

$$V_{C_1} = V_{L_2} \tag{2}$$

$$V_{C_2} = V_{L_3} \tag{3}$$

Fig. 3(c) explains the circuit diagram of CCBC in switch OFF mode. When S is turned OFF, the input capacitor C_{in} is charging with the DC input voltage V_{in}. This time the input inductor L_1 starts discharging through the diode D_1. The capacitors C_1 and C_2 are also in charging mode and hence the corresponding inductors L_2 and L_3 start releasing energies through the diode D_2 and D_0. Hence, the diodes D_1, D_2, and D_0 are forward biased and the diodes D_3 and D_4 are reverse biased. In this period, the output capacitor C_{dc} is storing energy. Applying KVL we get the following inductor voltage equations:

$$V_{in} - V_{C_1} = V_{L_1} \tag{4}$$

$$V_{C_1} - V_{C_2} = V_{L_2} \tag{5}$$

$$V_{C_2} - V_{C_{dc}} = V_{L_3} \tag{6}$$

Let the switching period be T, the turn-on duty cycle D and the turn-off duty cycle is $(1–D)$. Assuming all elements of the circuit are to be ideal and the inductor currents in a continuous conduction mode, applying the volt-second balance theorem for Eqs. (1)-(6), we obtain the following equations for one switching cycle:

$$V_{in}D + (V_{in} - V_{C_1})(1-D) = 0 \tag{7}$$

$$V_{C_1}D + (V_{C_1} - V_{C_2})(1-D) = 0 \tag{8}$$

$$V_{C_2}D + (V_{C_2} - V_{C_{dc}})(1-D) = 0 \tag{9}$$

From Eqs. (7), (8) and (9) we get:

$$\frac{V_0}{V_{in}} = \frac{1}{(1-D)^3} = G \tag{10}$$

where G is the DC voltage gain of the CCBC.

B. Design of Inductors

From Eqs. (1-3) we get the following equations:

$$V_{in} = L_1 \frac{dI_{L_1}}{dt} \tag{11}$$

$$V_{C_1} = L_2 \frac{dI_{L_2}}{dt} \tag{12}$$

$$V_{C_2} = L_3 \frac{dI_{L_3}}{dt} \tag{13}$$

From Eq. (11) we get the value of L_1,

$$\Delta I_{L_1} = \frac{V_{in}}{L_1} DT \tag{14}$$

Similarly, from Eqs. (12) and (13),

$$\Delta I_{L_2} = \frac{V_{C_1}}{L_2} DT \tag{15}$$

$$\Delta I_{L_3} = \frac{V_{C_2}}{L_3} DT \tag{16}$$

For continuous conduction mode,

$$\Delta I_{L_1(\min)} = I_{L_1} - \frac{1}{2}\Delta I_{L_1} \geq 0 \tag{17}$$

$$\Delta I_{L_2(\min)} = I_{L_2} - \frac{1}{2}\Delta I_{L_2} \geq 0 \tag{18}$$

$$\Delta I_{L_3(\min)} = I_{L_3} - \frac{1}{2}\Delta I_{L_3} \geq 0 \tag{19}$$

Let the current passing through the output diode D_0 connected to the load R be I_{dc}. Here, $I_{dc} = V_0/R$.

Hence,

$$I_{L_1} = \frac{V_0}{(1-D)^3 R} = \frac{V_{in}}{(1-D)^6 R} \tag{20}$$

$$I_{L_2} = \frac{V_0}{(1-D)^2 R} = \frac{V_{in} D}{(1-D)^5 R} \tag{21}$$

$$I_{L_3} = \frac{V_0}{(1-D)^4 R} = \frac{V_{in} D}{(1-D)^7 R} \tag{22}$$

Using Eqs. (11), (17) and (20) we get the value of inductor L_1:

$$L_1 \geq \frac{RD(1-D)^6}{2 f_s} \tag{23}$$

Similarly, using Eqs. (12), (18) and (21) we get the value of inductor L_2 :

$$L_2 \geq \frac{RD(1-D)^4}{2 f_s} \tag{24}$$

And, again using Eqs. (13), (19) and (22) we get the value of L_3 :

$$L_3 \geq \frac{RD(1-D)^7}{2 f_s} \tag{25}$$

C. Design of Capacitors:

During switch ON mode,

$$I_{C_1} = I_{L_2} \tag{26}$$

Implementing I_{L_2} from Eqs. (21) in (26),

$$I_{L_2} = \frac{V_0}{R}(1-D)^2 = C_1 \frac{dV_{C_1}}{dt}$$

Hence,

$$C_1 = \frac{V_0 D}{R\Delta V_{C_1} f_s (1-D)^2} \tag{27}$$

Similarly, the design parameter of capacitors C_2 and C_{dc} using Eqs. (14) and (16) can be obtained:

$$C_2 = \frac{V_0 D}{R\Delta V_{C_2} f_s (1-D)^3} \tag{28}$$

$$C_{dc} = \frac{V_0 D}{R\Delta V_{C_3} f_s (1-D)^4} \tag{29}$$

Here, f_s=1/T is the switching frequency of the CCBC.

The corresponding inductor waveforms for the CCBC circuit obtained from mathematical and simulated analysis are shown in Fig.4 (a) and (b). Assuming all the switches and passive elements of the circuit are ideal, the DC voltage gain for CCBC has been calculated in Eq. (10). A comparison analysis between mathematically calculated output voltage as mentioned in Eq. (10) and simulated output voltage of CCBC with varying duty cycle is shown in Fig. 5 using a resistive load R = 400 Ω, Fig. 6 shows various step-up DC-DC converter voltage gain ratios varied with the duty cycle found in the literature mentioned in [10–14]. The results show that CCBC has a higher voltage gain among all.

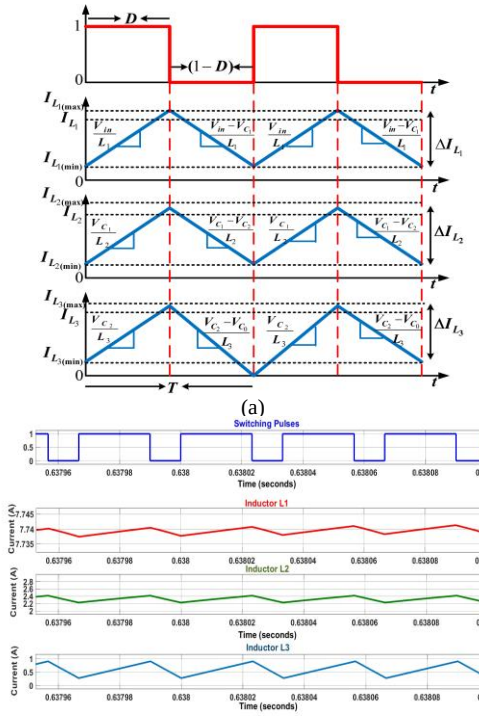

(a)

(b)

Fig. 4. CCBC operating characteristics waveforms for inductors: (a) mathematical (b) simulated.

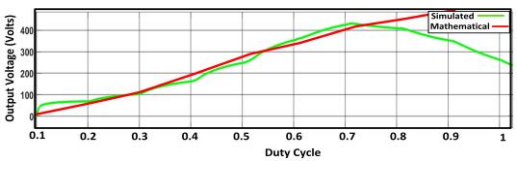

Fig. 5 Comparison of output voltage variation with varying duty cycle of the CCBC with simulated and mathematical analysis.

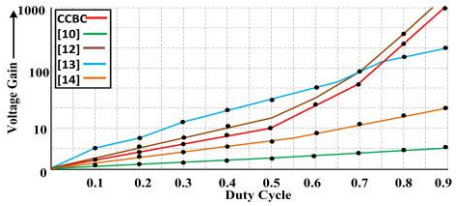

Fig. 6. Comparison of voltage gain with duty cycle of the CCBC for the proposed combination with other converter topologies.

TABLE I: SIMULATION SPECIFICATIONS FOR THE PROPOSED SYSTEM

PV Panel specifications		CCBC Specifications		LCL filter Specifications	
Parameters	Value	Parameters	Value	Parameters	Value
Maximum power (P_{max})	229.99 W	L_1	100 μH	L_a	1000 μH
Voltage at MPP (V_{max})	29.6 V	L_2	100 μH	L_b	1000 μH
Current at MPP (I_{max})	7.77 A	L_3	100 μH	L_c	1000 μH
Short circuit current (I_{SC})	8.63 A	C_1	100 μF	L_{ga}	500 μH
Open Circuit Voltage (V_{OC})	36.8 V	C_2	100 μF	L_{gb}	500 μH
Cell per module	60	C_{dc}	3225 μF	L_{gc}	500 μH
Diode ideality factor	0.948	Switching frequency (f_s)	30,000 Hz	C_c	100 μF
Shunt resistance	63.82 Ω	Duty cycle (D)	40–70%	C_a	100 μF
Input PV voltage at MPP	120 V	Output voltage	820–1230 V	C_b	100 μF
Input PV current at MPP	23–46 A	Output current	3.1–4.3 A	R	400 Ω

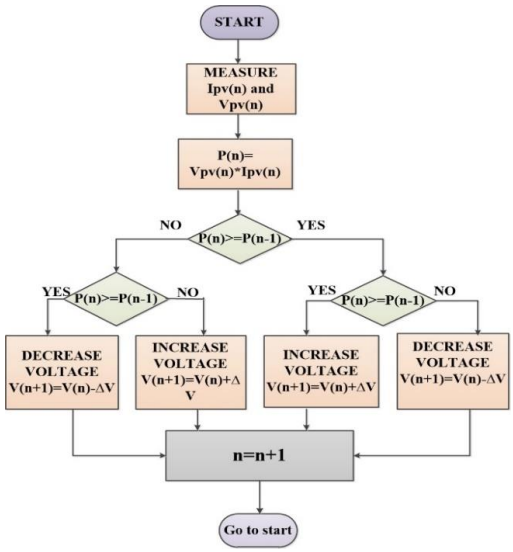

Fig. 7. Flowchart of P&Q MPPT algorithm.

D. P&O Maximum Power Point Tracking (MPPT)

PV arrays contain an MPPT point depending on their *I-V* characteristics. Table I gives information about the rated parameter value of the PV panels used in the proposed combination. To receive the maximum available power from the PV panels, MPPT algorithms have been implemented with the converter control. There are various direct and indirect MPPT algorithms in the literature. Among them, P&O is the most dominantly used MPPT method on account of its simplicity [20]. Fig. 7 shows the flow chart for the P&O algorithm. This algorithm finds maximum power by increasing the voltage or currents obtained from PV panels unless it reaches the maximum point.

This algorithm works on employing perturbation to the PV voltage or PV current in which the converter is operated using the samples of voltage $V_{pv}(n)$ and current $I_{pv}(n)$ following the variation in the operating power [21]. After reaching the maximum point, the algorithm measures the current power point with the previous one and if it is lower than the previous point it further increases the voltage until it reaches the maximum point. P&O can be classified into fixed-step P&O and variable-step P&O algorithms. In fixed step P&O MPPT, there is a fixed point set by the PI controller and the voltage or current reference has been taken to reach the maximum power point [20, 21]. In the variable P&O algorithm, derivatives of the ratio of power to voltage or current are utilized. PI controller used in P&O MPPT algorithms gives a more stable control in the converter output compared to the other algorithms found in literature such as Hill climbing and direct control algorithm which do not employ a PI controller.

In this paper, a fixed-step P&O algorithm is used considering its simplicity and the advantage of fixed set MPPT points. While implementing in MATLAB/ SIMULINK, the frequency for the triangular wave is taken as 500 Hz and the duty cycle adjusting range is between 0.40 and 0.75.

III. THE INVERTER ANALYSIS

The DC bus voltage of the CCBC is further connected to a three-phase full bridge inverter as shown in Fig. 8. The DC link capacitor C_{dc} provides the required input voltage for the inverter. It is connected further to the grid via LCL filter with a balanced star-connected resistive load. The inverter consists of three legs of six high frequency IGBTs labelled as Q_1 to Q_6. Let the Per phase voltages are V_a, V_b, and V_c, and currents are I_a, I_b, and I_c respectively and V_o is the neutral voltage.

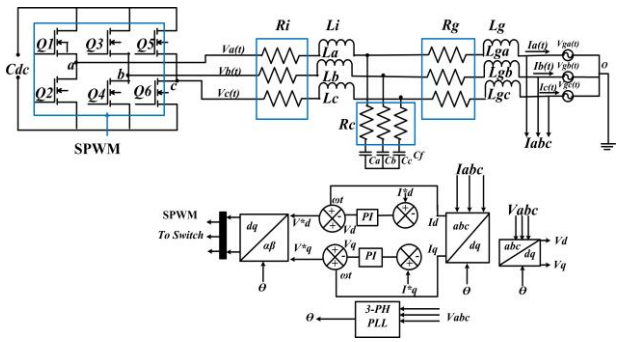

Fig. 8. Three phase full bridge inverter circuit diagram presenting the LCL filter and *dq* control scheme.

Let the LCL filter has the inverter side equivalent inductance L_i and the grid side equivalent inductance L_g. C_f acts for the equivalent capacitance of LCL filter. V_{ga}, V_{gb} and V_{gc} and I_{ga}, I_{gb} and I_{gc} are the grid side voltages and currents per phase of the grid utility. R is the sum of inverter side equivalent resistance (R_i) and the grid side equivalent resistance (R_g) of the LCL filter inductors. R_c is the equivalent series resistance of the capacitors used in LCL filters.

A. Per Phase Analysis

Using KVL in Fig. 8, we get the following equations [22]:

$$L_a \frac{dI_a}{dt} + R(t) = V_a - V_o \tag{30}$$

$$L_b \frac{dI_b}{dt} + R(t) = V_b - V_o \tag{31}$$

$$L_c \frac{dI_c}{dt} + R(t) = V_c - V_o \tag{32}$$

Again, for a balanced load,

$$I_a + I_b + I_c = 0 \tag{33}$$

Hence, by adding Eqs. (30), (31), (32) and (33) we get,

$$V_o = \frac{V_a + V_b + V_c}{3} \tag{34}$$

By substituting Eq. (34) in Eqs. (30), (31) and (32) respectively and using the criteria of (33) we get,

$$\left.\begin{aligned} L_a \frac{dI_a}{dt} + R(t) &= \frac{1}{3}\left(V_{ab}(t) - V_{ac}(t)\right) \\ L_b \frac{dI_b}{dt} + R(t) &= \frac{1}{3}\left(V_{ab}(t) - V_{bc}(t)\right) \\ L_c \frac{dI_c}{dt} + R(t) &= \frac{1}{3}\left(V_{ac}(t) - V_{bc}(t)\right) \end{aligned}\right\} \tag{35}$$

Eq. (35) establish a relationship between per-phase currents and line voltages of the inverters. Hence, these equations are the analytical calculations for the phase-currents that can be analytically used to optimize the harmonic performance of the inverter [23]. The equations for phase current detection are as follows:

$$\left.\begin{aligned} I_a(t) &= \frac{1}{3}\left(I_{ab}(t) + I_{ac}(t)\right) \\ I_b(t) &= \frac{1}{3}\left(I_{bc}(t) + I_{ab}(t)\right) \\ I_c(t) &= \frac{1}{3}\left(I_{ac}(t) + I_{bc}(t)\right) \end{aligned}\right\} \tag{36}$$

In a balanced condition, the following equations can be obtained from the proposed system:

$$V_{ga} + V_{gb} + V_{gc} = 0 \tag{37}$$

$$L_a + L_b + L_c = 0 \tag{38}$$

$$L_{ga} + L_{gb} + L_{gc} = 0 \tag{39}$$

To eliminate the leakage current that has been formed by the parasitic capacitance of the PV array and ground in a transformerless PV system, a filter-clamped topology is used with the full bridge inverter by clamping the LCL filter output to the midpoint of the DC bus [24]. In the proposed work calculations for leakage current have not been accounted for.

B. Control Scheme

To provide control to the power switches used in the inverter circuit, an active and reactive power (*dq*) control scheme is introduced. By this control method, the fundamental positive and negative sequence components of instantaneous current I_d and I_q can be separated [25]. In this method, the load current of the system is transformed from the *abc* stationary reference frame to the *dq* synchronous reference frame [26].

The first step is *abc* to *dq* transformation where the output voltage and current of the three-phase inverter are converted into two-phase quantity. In the second step, grid side voltage and current are detected using a phase-lock-loop (PLL) where active and reactive power for the inverter and the grid have been calculated and the values are tuned using PI controllers. The *dq* voltage and current quantity are processed via the PI controller and generate SPWM control logic for the three-phase inverter by comparing the PWM pulses with a triangular wave. The switching frequency used for the three-phase inverter is 10kHz and grid side frequency 50Hz. The simulation steps of the *dq* control scheme used in the inverter circuit for the proposed combination are explained in Fig. 9.

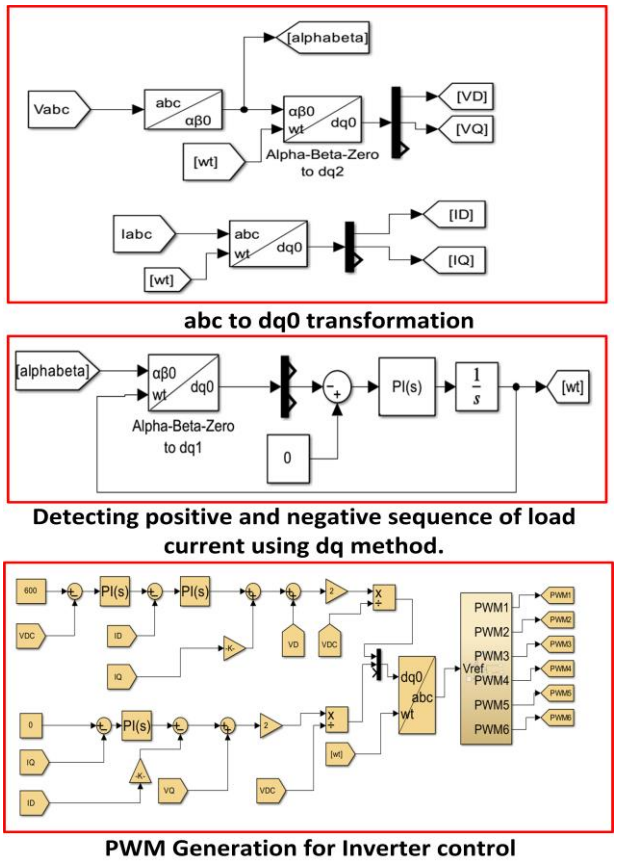

Fig. 9. Simulink design of *dq* controller for the three phase inverter.

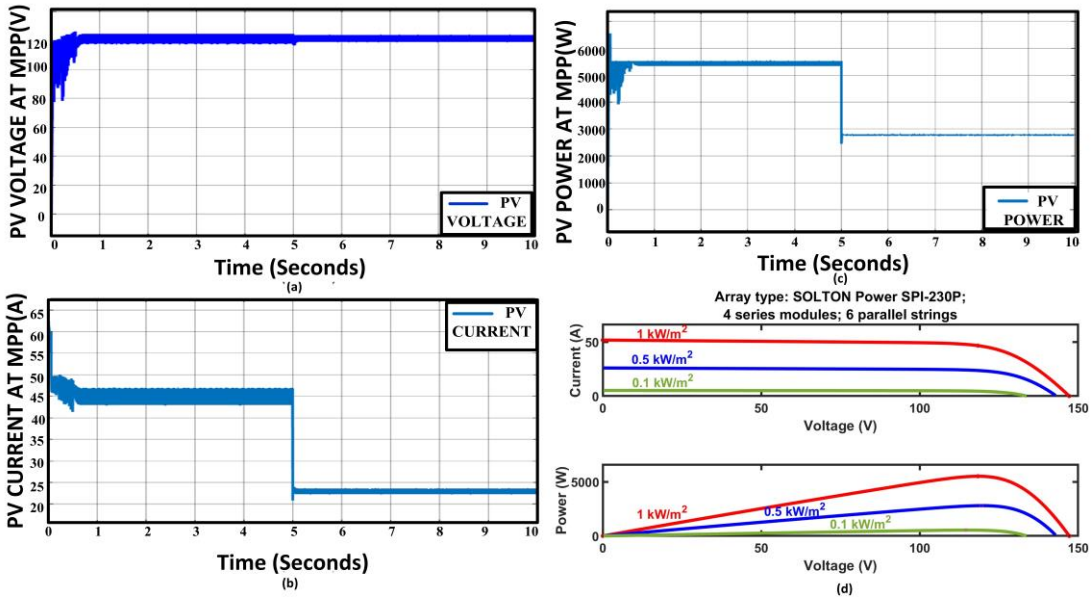

Fig. 10. Simulated characteristics waveforms: (a) PV voltage at MPP vs time, (b) PV current at MPP vs time, (c) PV power at MPP vs time, and (d) PV Panel characteristics at various MPPs.

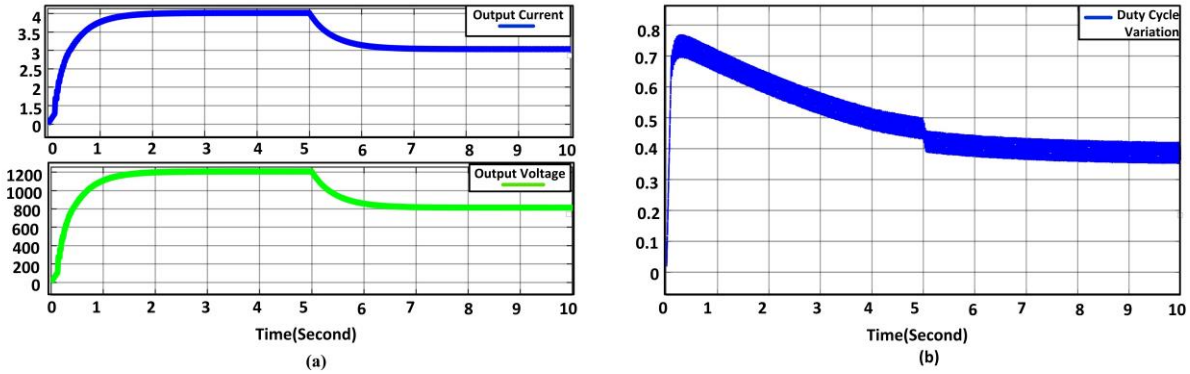

Fig. 11. Simulated waveforms: (a) CCBC output current and voltage characteristics of dynamic responses in varying irradiance condition and (b) variation of duty cycle.

IV. System Simulation and Analysis of Result

The proposed combination is simulated in MATLAB/ SIMULINK employing a 5.5 kW PV source for a time period of 10 seconds: (a) first 5 seconds in 1000 W/m^2; (b) last 5 seconds in 500 W/m^2 irradiance level. Four series modules and six parallel strings of SOLTON POWER SPI-230P PV panels are selected for simulation. Parameters specifications for PV panels, circuit elements of CCBC and LCL filters are given in Table 1. The DC bus voltage is significantly maintained by the P&O MPPT controller around the reference point under variable irradiance. The simulated characteristics waveforms for PV voltage, PV current and PV power at maximum power point (MPP) with change in irradiance level (step change in 5 second from 1000 W/m^2 to 500 W/m^2) are shown in Fig. 10(a), (b) and (c) respectively. The maximum generated PV power is 5.5 kW in 1000 W/m^2 and 2.8 kW in 500 W/m^2 irradiance level while the PV voltage is 120V and PV current is between 23 A to 46 A at MPP. The SOLTON POWER SPI-230P PV panel characteristics at various MPPs and its corresponding voltage, current and power are shown in Fig.10 (d). From the simulated waveforms of Fig. 11(a) and (b), it is observed that varying the cycle between 40% to 75%, the CCBC converter can deliver a stable DC bus voltage of 1230V with 4.3A output current at 1000 W/m^2 and 820 V with 3.1 A output current at 500 W/m^2. Hence the CCBC is capable of providing a high boosting and robust control around MPP proving its suitability for PV application.

The inverter output voltage and output current of the proposed combination are shown in Fig. 12(a) and (b) respectively. The inverter itself produces and maintains a 399 V peak and 230 V RMS voltage in each phase from an 820 V to 1230 V DC bus under variable irradiance. The current output is 12.6 A peak and 7.3 A RMS per phase for 1000 W/m^2 and 6 A peak and 3.5 A RMS per phase for 500 W/m^2. The inverter power delivered is 5.03 kW. The grid voltage and the grid current are shown in Fig. 12(c) and (d). The system maintains a grid voltage of a constant 230 V RMS per phase under variable irradiance. The SPWM signal generated for the six switches of inverter is shown in Fig. 13. The proposed combination is worked on unity power factor by producing 2.4 kW to 5.03 kW of active power and –220 to –295 VAR reactive power considering variable irradiance as shown in Fig. 14.

The inverter current THD as shown in Fig. 15 is calculated for the proposed combination shows 1.91% (<5% according to IEEE standard range for inverter THD).

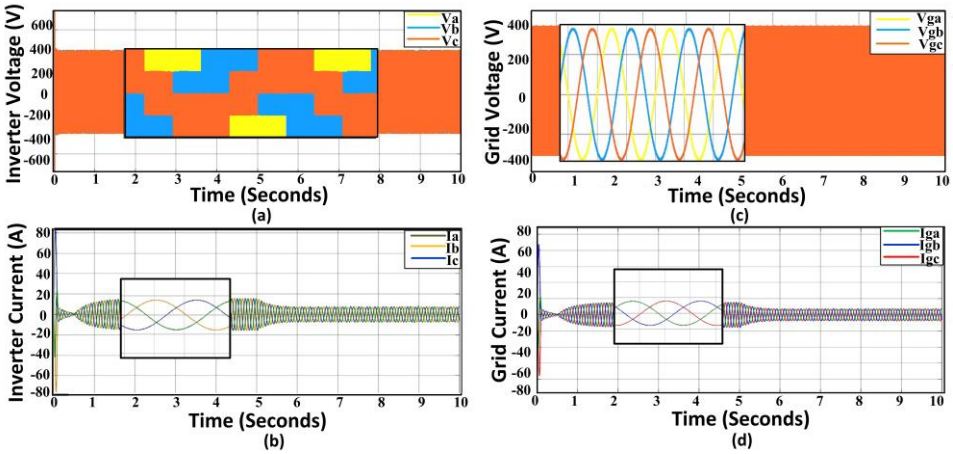

Fig. 12. Simulate (a) inverter voltage (b) inverter current (c) grid voltage (d) grid current.

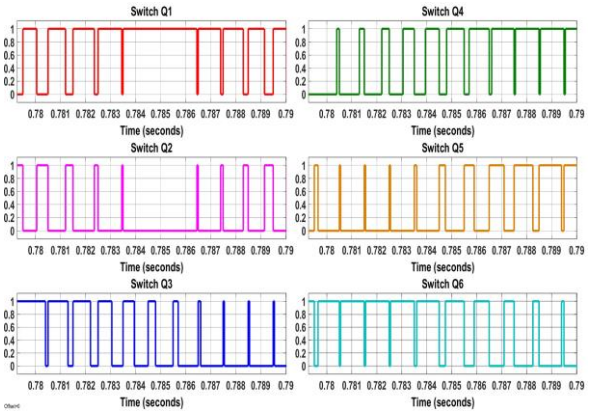

Fig. 13. SPWM Signal generated for inverter switches.

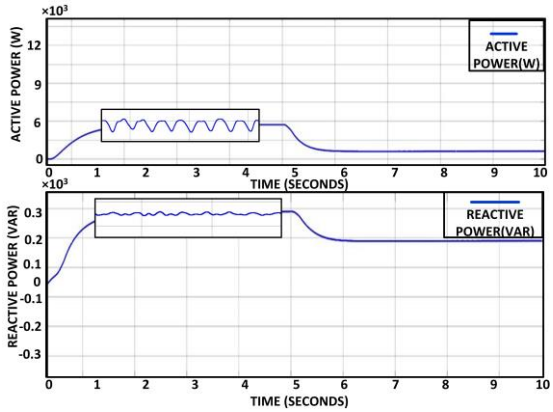

Fig. 14. Simulated power: (a) Active power (b) reactive power.

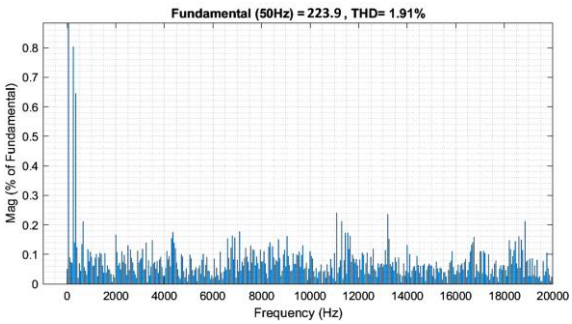

Fig. 15. Analysis of Inverter current THD in steady state.

The input inductor ripple currents and the output capacitor ripple voltages are plotted in Fig. 16 by varying the irradiance level from 100 W/m^2 to 1000 W/m^2. The result shows a very lower amount of ripple obtained in accordance with the lower irradiance level to the higher irradiance level despite the unstable and noise full characteristics of the PV source. The variation of ripple with irradiance in terms of input current is almost constant and output voltage ripple variation is also negligible (between 4–6 V). A brief analysis of the result of the proposed combination is tabulated in Table 2 showing the maximum power, voltage and current available in the inverter output side and the power factor, THD and the system efficiency. The proposed combination is suitable for grid utilization as it provides high voltage DC bus with lesser voltage ripple and lower AC fluctuation tracing zero even harmonics in inverter output in a rated grid output voltage.

TABLE II: ANALYSIS OF RESULTS

Parameters	Maximum Value Obtained
RMS output power	5.03 kW
Peak output voltage	399 V(Peak)
Peak output current	12.6 A(Peak)
RMS output voltage	230 V
RMS output current	7.3 A
Power factor	1
THD	1.91%
Efficiency	91%

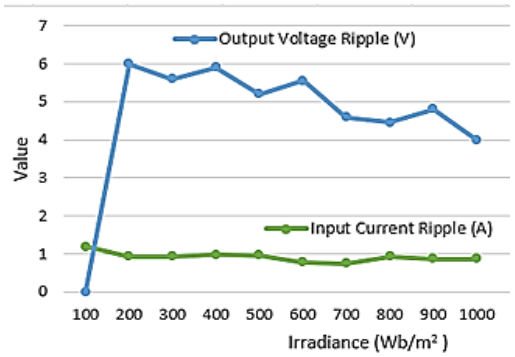

Fig. 16. Input ripple current and output ripple voltage w.r.t variable irradiance.

The high voltage gain, lower ripple and the lower inverter THD is the main provision of the proposed combination that can provide bulk power to the utility grid. The proposed combination is suitable for low voltage PV applications and for household PV systems. Moreover, the employment of other efficient inverters such as Z-source inverters, H-bridge inverters and multilevel inverters may be utilized with the CCBC for PV applications to obtain high efficiency and enhanced power density.

V. Conclusion

In two stage PV system, an MPPT controller-based DC-DC converter is necessary to provide a stable, less noise and ripple-free DC link voltage input to the inverter by pulling out maximum power from the PV panel. In this paper, an improved highly efficient boost converter employing a diode-capacitor-inductor based cubic cell is used with the well-established 3-ph conventional inverter topology and the simulated results present that the proposed combination is suitable for PV applications. The CCBC can be improved to have less voltage stress on the DC link capacitor using a switched capacitor and diode arrangement without any complex control. The proposed system is well-suited using *dq* control for grid requirement fulfillment with unity power factor and low AC harmonics. For a transformerless PV system, the leakage current is generated between the PV panel and the ground. As a future work, an experimental setup may be established for this proposed combination to analyze the dynamic performances of the system accounting for the leakage current.

Conflict of Interest

The authors declare no conflict of interest.

Author Contributions

The concept, investigation, circuit analysis, software simulation, manuscript preparation and review editing have been done by Anjana Saikia. The guidance, supervision and validation of the proposed work have been done by Santanu Sharma. All authors have approved the final version.

References

[1] B. Stevanovic, E. Serban, S. Cobreces, P. Alou, M. Ordonez, and M. Vasic, "DC/DC stage contribution to bus voltage in 1000-and 1500-V grid-connected solar inverters," *IEEE J Emerg. Sel. Top. Power Electron.*, vol. 10, no. 5, 2022, doi: 10.1109/JESTPE.2022.3175950

[2] K. Zeb, W. Uddin, M. A. Khan *et al.*, "A comprehensive review on inverter topologies and control strategies for grid connected photovoltaic system," *Renewable and Sustainable Energy Reviews*, vol. 94. pp. 1120–1141, Oct. 2018.

[3] M. Merai, M. W. Naouar, I. Slama-Belkhodja, E. Monmasson," A systematic design methodology for DC-link voltage control of single-phase grid-tied PV systems,", *Mathematics and Computers in Simulation*, vol. 183, 2021, pp. 158-170, 2021, doi: 10.1016/j.matcom.2020.05.007

[4] N. Tak, S. K. Chattopadhyay and C. Chakraborty, "Single-sourced double-stage multilevel inverter for grid-connected solar PV systems," *IEEE Open Journal of the Industrial Electronics Society*, vol. 3, pp. 561-581, 2022

[5] S. Alotaibi and A. Darwish, "Modular multilevel converters for large-scale grid-connected photovoltaic systems: A review," *Energies*, vol. 14, no. 19, #6213, Sep. 2021.

[6] P. Chouhan, A. Chourey, and B. Yadav, "Performance analysis of grid tied three phase single stage and dual stage PV system; A review paper," *Journal for Research*, vol. 7, 2021, [Online]. Available: www.journal4research.org

[7] M. H. Nguyen and K. K. Ahn, "An improved voltage regulation performance of floating interleaved boost converters for fuel cell applications subject to input variation and load change," *Applied Sciences*, vol. 12, no. 22, #11501, Nov. 2022.

[8] R. Kumar, R. Kannan, N. B. M. Nor, and A. Mahmud, "A high step-up switched Z-source converter (HS-SZC) with minimal components count for enhancing voltage gain," *Electronics*, vol. 10, no. 8, #924, Apr. 2021.

[9] B. Stevanovic, Di. Serrano, M. Vasic, P. Alou, J. A. Oliver, and J. A. Cobos, "Highly efficient, full ZVS, hybrid, multilevel DC/DC topology for two-stage grid-connected 1500-V PV system with employed 900-V SiC devices," *IEEE J Emerg. Sel. Top. Power Electron.*, vol. 7, no. 2, pp. 811–832, Jun. 2019.

[10] Z. Liao, Y. Lei, and R. C. N. Pilawa-Podgurski, "Analysis and design of a high-power density flying-capacitor multilevel boost converter for high step-up conversion," *IEEE Trans Power Electron*, vol. 34, no. 5, pp. 4087–4099, May 2019.

[11] Y. Jiang, M. K. Law, Z. Chen, P. I. Mak, and R. P. Martins, "Algebraic series-parallel-based switched-capacitor DC-DC boost converter with wide input voltage range and enhanced power density," *IEEE J. Solid-State Circuits*, vol. 54, no. 11, pp. 3118–3134, Nov. 2019.

[12] Y. Hao, K. Guo, L. Liu, W. Cai, and F. Liu, "Improved cubic boost converter based on voltage closed-loop control," *Energy Reports*, vol. 8, pp. 87–95, Sep. 202.

[13] A. Alzahrani, P. Shamsi, and M. Ferdowsi, "Interleaved multistage step-up topologies with voltage multiplier cells," *Energies (Basel)*, vol. 13, no. 22, Nov. 2020, doi: 10.3390/en13225990.

[14] S. Alotaibi, A. Darwish, and B. W. Williams, "Three-phase inverter based on isolated SEPIC/CUK converters for large-scale PV applications," *International Journal of Electrical Power and Energy Systems*, vol. 146, Mar. 2023, doi: 10.1016/j.ijepes.2022.108723.

[15] L. Monjo, L. Sainz, J. J. Mesas, and J. Pedra, "Quasi-Z-source inverter-based photovoltaic power system modeling for grid stability studies," *Energies*, vol. 14, no. 2, #508, Jan. 2021.

[16] M. Venkatesan, R. Rajeswari, M. Kaliyamoorthy, and M. Srithar, "Transient and steady state analysis of modified three phase multilevel inverter for photovoltaic system," *International Journal of Power Electronics and Drive System (IJPEDS)*, vol. 8, no. 1, pp. 31–39, 2017.

[17] H. T. Nguyen, E. K. Kim, I. P. Kim, H. H. Choi, and J. W. Jung, "Model predictive control with modulated optimal vector for a three-phase inverter with an LC filter," *IEEE Trans Power Electron*, vol. 33, no. 3, pp. 2690–2703, Mar. 2018.

[18] M. R. Chen, H. Wang, G. Q. Zeng, Y. X. Dai, and D. Q. Bi, "Optimal P-Q control of grid-connected inverters in a microgrid based on adaptive population extremal optimization," *Energies (Basel)*, vol. 11, no. 8, 2018, doi: 10.3390/en11082107.

[19] M. H. Mondol, M. R. Tür, S. P. Biswas, M. K. Hosain, S. Shuvo, and E. Hossain, "Compact three phase multilevel inverter for low and medium power photovoltaic systems," *IEEE Access*, vol. 8, pp. 60824–60837, 2020, doi: 10.1109/ACCESS.2020.2983131.

[20] Zaheeruddin, S. Mishra, and A. Haque, "Performance evaluation of modified perturb & observe maximum power point tracker for solar PV system," *International Journal of System Assurance Engineering and Management*, vol. 7, 2016, doi: 10.1007/s13198-015-0369-z.

[21] S. Motahhir, A. El Hammoumi, and A. El Ghzizal, "The most used MPPT algorithms: Review and the suitable low-cost embedded board for each algorithm," *Journal of Cleaner Production*, vol. 246, 2020. doi: 10.1016/j.jclepro.2019.118983.

[22] A. K. Singh, S. Kumar, and B. Singh, "Solar PV energy generation system interfaced to three phase grid with improved power quality," *IEEE Transactions on Industrial Electronics*, vol. 67, no. 5, 2020, doi: 10.1109/TIE.2019.2921278.

[23] S. Tyagi and I. Mayergoyz, "Optimal time-domain pulse width

modulation for three-phase inverters," *AIP Advances*, vol. 10, no.2, 2020, doi: http://doi.org/10.1063/1.5134774.
[24] T. Kerekes, R. Teodorescu, M. Liserre, C. Klumpner, and M. Sumner, "Evaluation of three-phase transformerless photovoltaic inverter topologies," *IEEE Trans Power Electron*, vol. 24, no. 9, pp. 2202–2211, 2009.
[25] T. D. Gupta, D. Kumar, and K. Chaudhary, "Modelling and analysis of grid-tied fuel cell system with synchronous reference frame control," in *Proc. of 2017 4th International Conference on Power, Control and Embedded Systems*, 2017, doi: 10.1109/ICPCES.2017.8117665.
[26] A. Darwish, D. Holliday, S. Ahmed, A. M. Massoud, and B. W. Williams, "A single-stage three-phase inverter based on cuk converters for PV applications," *IEEE Journal of Emerging and Selected Topics in Power Electronics*, vol. 2, no. 4, pp. 797–807, 2014.

Anjana Saikia received a BTech degree in Electrical and Electronics Engineering from North Eastern Hill University, Shillong, India in 2015 and her MTech degree in Electrical Power System Engineering from North Eastern Regional Institute of Science and Technology, Arunachal Pradesh, India in 2018. She is currently pursuing her Ph.D. degree at the Department of Electronics and Communication Engineering, Tezpur University, India. Her area of research includes power electronics converters and power electronics interfaces in photovoltaic (PV) microgrids.

Santanu Sharma received his B.E degree in Electrical Engineering from Jorhat Engineering College, Jorhat, India in 1998 and his MTech degree in 2000 with a specialization in Electronics Devices & Technology (ELDT) from Tezpur University, India. He holds his Ph.D. degree in 2010 from Tezpur University and currently, he is securing the position of HOD and Professor at the Department of Electronics and Communication Engineering, Tezpur University. His research interests include semiconductors, Bioelectronic devices, Power Electronics, Traction control in Electric vehicles etc. He can be contacted at email: santanu.sharma@gmail.com.